

H α observations of the γ -ray-emitting Be/X-ray binary LSI+61⁰303: orbital modulation, disk truncation, and long-term variability \star

R. Zamanov¹, K. Stoyanov¹, J. Marti², N. A. Tomov¹, G. Belcheva^{3,4}, P. L. Luque-Escamilla⁵, and G. Latev¹

¹ Institute of Astronomy and National Astronomical Observatory, Bulgarian Academy of Sciences, 72 Tsarigradsko Shousse Blvd., 1784 Sofia, Bulgaria

e-mail: rkz@astro.bas.bg, kstoyanov@astro.bas.bg, jmarti@ujaen.es, tomov@astro.bas.bg

² Departamento de Física (EPSJ), Universidad de Jaén, Campus Las Lagunillas, A3-420, 23071, Jaén, Spain

³ Department of Astronomy, St. Kliment Ohridski University of Sofia, 5 James Bourchier Blvd., 1164 Sofia, Bulgaria

⁴ Department of Physics and Astronomy, Pevensey II Building, University of Sussex, Falmer, Brighton BN1 9QH, UK

⁵ Departamento de Ingeniería Mecánica y Minera (EPSJ), Universidad de Jaén, Campus Las Lagunillas A3-008, 23071, Jaén, Spain

Received May 30, 2013; accepted September 12, 2013

ABSTRACT

We report 138 spectral observations of the H α emission line of the radio- and γ -ray-emitting Be/X-ray binary LSI+61⁰303 obtained during the period of September 1998 – January 2013. From measuring various H α parameters, we found that the orbital modulation of the H α is best visible in the equivalent width ratio $EW(B)/EW(R)$, the equivalent width of the blue hump, and in the radial velocity of the central dip. The periodogram analysis confirmed that the H α emission is modulated with the orbital and superorbital periods. For the past 20 years the radius of the circumstellar disk is similar to the Roche lobe size at the periastron. It is probably truncated by a 6:1 resonance. The orbital maximum of the equivalent width of H α emission peaks after the periastron and coincides on average with the X-ray and γ -ray maxima.

All the spectra are available upon request from the authors and through the CDS.

Key words. Stars: individual: LSI+61⁰303 – X-rays: binaries – Stars: winds, outflows

1. Introduction

The Be/X-ray binary LSI+61⁰303 was first detected as strong γ -ray source with COS B (Hermsen et al. 1977) and as an X-ray source with the *Einstein* observatory (Bignami et al. 1981). The Be/X-ray binaries (BeXRB) are systems that consist of a compact object that orbits an optical companion. The optical companion is a Be star. Be stars are non-supergiant fast-rotating B-type and luminosity class III-V stars that at some point of their lives have shown spectral lines in emission (Porter & Rivinius 2003; Balona 2000; Slettebak 1988). The best-studied lines are those of hydrogen (Balmer and Paschen series), but the Be stars can also show He and Fe in emission (see Hanuschik 1996 and references therein). They also show some infrared excess. The origin of the emission lines and infrared excess in BeXRB is attributed to an equatorial disk that is fed from material expelled from the rapidly rotating Be star. During periastron, the compact object passes close to this disk, sometimes may even go through it and cause a major disruption. A strong flow of matter is then captured by the compact object. In most cases the compact object is a neutron star (NS) detected as an X-ray pulsar (Bildsten et al. 1997 and references therein). The conversion of the kinetic energy of the infalling matter into radiation powers the X-rays.

The high-mass X-ray binary LS I +61⁰ 303 (V615 Cas) is known as a variable radio source (Gregory et al. 1979) characterized by nonthermal periodic radio outbursts (Gregory & Taylor 1978). Its energetic outbursts are also visible in X-rays (Greiner

& Rau 2001, Harrison et al. 2000), and GeV wavelengths (Abdo et al. 2009, Albert et al. 2008, Acciari et al. 2008). The system has a relatively low X-ray luminosity for a high-mass X-ray binary, but is one of the 20 brightest γ -ray sources known and detectable up to TeV energy range. It is one of only few such systems identified as a source of TeV gamma rays. Indeed, it is currently considered to be a member of the new class of gamma-ray-emitting binaries, that is binary systems whose luminosity output has a dominating component at gamma-ray energies (see e.g. Paredes et al. 2013).

LSI+61⁰303 consists of a massive B0Ve star and a compact object. The nature of the compact object remains a mystery even after four decades of observations over a wide range of wavelengths. Most probably it is a magnetic neutron star, but it might be a magnetized black hole (Punsly 1999) acting as a precessing microblazar (Massi, Ros & Zimmermann 2012). The compact object moving in an eccentric orbit interacts with the Be circumstellar disk, producing strong orbital modulation in the emission across the electromagnetic spectrum: radio flux (Gregory & Taylor 1978; Taylor et al. 1992), X-ray (Paredes et al. 1997; Leahy 2001), optical V magnitude (Mendelson & Mazeh 1994, Zaitseva & Borisov 2003), TeV (Albert et al. 2006, 2008), and optical H α emission line (Zamanov et al. 1999, Grundstrom et al. 2007a). The radio morphology of the system also shows unique characteristics. The resolved extended structure changes position angle with a surprisingly large variation (Massi et al. 2004).

The motion on the sky determined with high precision astrometry implies that LSI+61⁰303 was ejected from the stellar

\star based on observations obtained at the National Astronomical Observatory Rozhen, Bulgaria

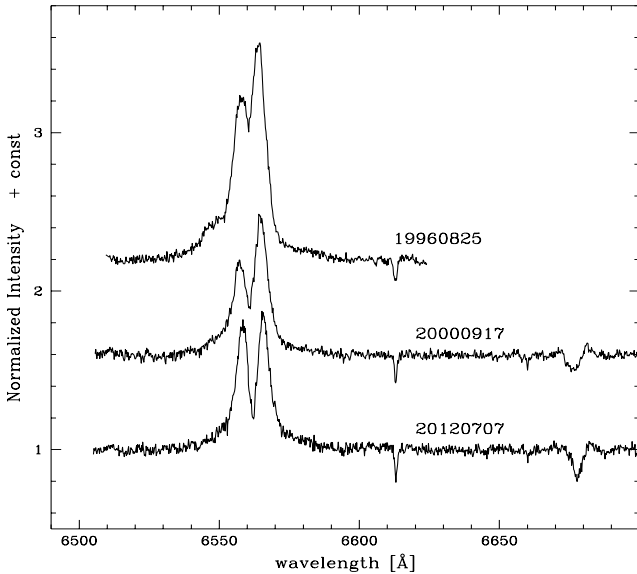


Fig. 1. Three examples of $H\alpha$ profiles. The upper spectrum is taken from the time of maximal $EW=18.2$ Å (19960825). The middle spectrum has a $EW=13.1$ Å (2000917). The lower spectrum (20120707, $EW=10.8$) is taken at a moment when the star fulfilled the shell criterion (see also Sect. 5.3).

cluster IC 1805 by the kick imparted to the compact object in an asymmetric supernova explosion $\sim 1.7 \times 10^6$ yr ago (Mirabel, Rodrigues, & Liu, 2004).

Additionally to the 26.5 d orbital modulation, a 4.4 yr periodic modulation of the phase and amplitude of the radio outbursts has been discovered (Paredes et al 1987; Gregory et al. 1989). This superorbital modulation has been detected in $H\alpha$ (Zamanov et al. 1999). The first clues that the 4 yr modulation is also visible in X-rays have been given by Apparao (2001), and are now confirmed by Li et al. (2012) using the longest monitoring performed to date by the Rossi X-ray Timing Explorer (RXTE).

In this paper we present $H\alpha$ observations of LSI +61° 303 obtained during the past 15 years, and discuss disk truncation, long-term variability, orbital modulation, and connection with high-energy emission.

2. Observations

All data reported here were obtained by the 2.0m RCC telescope of the National Astronomical Observatory Rozhen located in the Rhodope mountain range, Bulgaria. The star LSI+61°303 was observed between September 1998 and January 2013 with the Coudé spectrograph of this telescope. The spectra cover 200 Å around $H\alpha$, with a resolution of 0.2 Å pixel $^{-1}$.

The spectra were reduced in the standard way including bias removal, flat-field correction, wavelength calibration, and correction for the Earth's motion. Pre-processings and measurements were performed using various routines provided by IRAF. The spectra obtained within each observational night were processed and measured independently.

Table 1 lists the spectrum ID (the first six digits corresponding to the date - YYYYMMDD), JD of the start of the exposure, exposure time in minutes, signal-to-noise ratio (S/N) calculated for the continuum in the wavelength range 6620 - 6655 Å. On each spectrum we measured the total equivalent width of the $H\alpha$ emission line, hereafter EW , the heliocentric radial veloc-

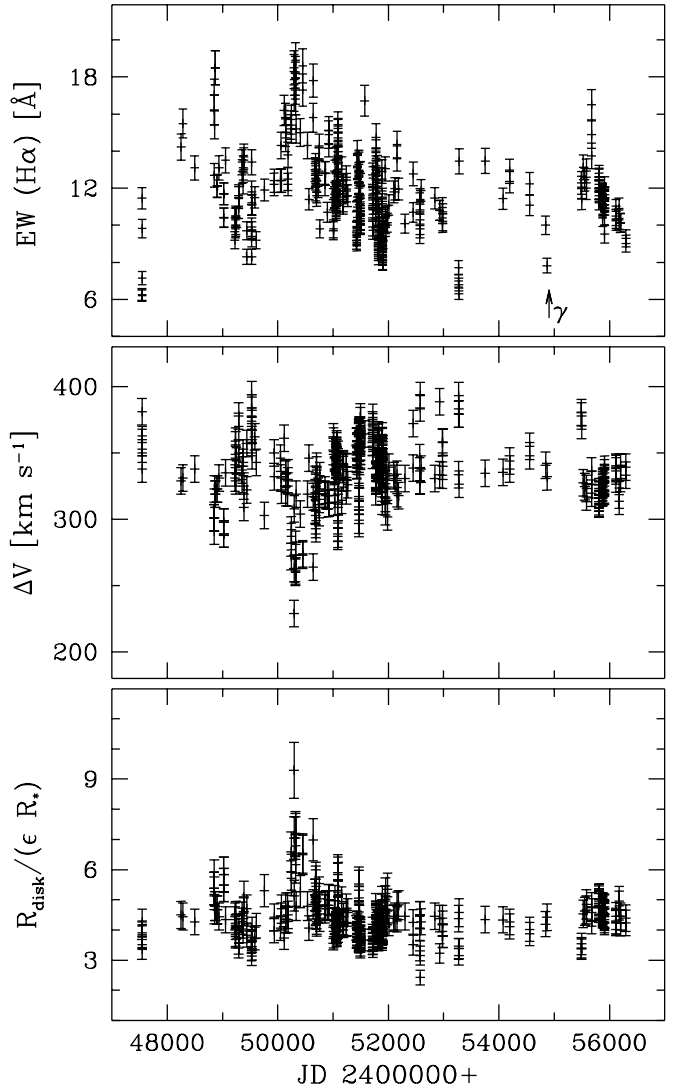


Fig. 2. Long-term variability of the equivalent width $EW(H\alpha)$, the distance between the peaks of the $H\alpha$ emission line, and the calculated radius of the $H\alpha$ -emitting circumstellar disk. The arrow in the upper panel corresponds to the time of the γ -ray flux transition (see also Sect.5.4.1).

ities of the central dip $V_r(cd)$, blue and red humps, $V_r(B)$ and $V_r(R)$ respectively, the ratio between the equivalent widths of the blue and red humps, the intensity of the blue peak I_B , the intensity of the red peak I_R , and the intensity of the central depression I_{cd} . The intensities were measured after normalization to the local continuum, $I_C \equiv 1$. The B/R ratio was calculated as $B/R = I_B/I_R$ (this ratio is more often called V/R ratio, but most of the papers on LSI+61°303 use B/R). The equivalent width of the blue hump, $EW(B)$, was measured from the violet end to the central dip. The equivalent width of the red hump, $EW(R)$, was measured from the central dip to the red end of the line, in this way: $EW = EW(B) + EW(R)$. We also give radial velocity of the HeI λ 6678.151 absorption line. The radial velocities were measured by employing a Gaussian fit. The errors depend mostly on the S/N, and we estimated them to be about 5% for EW , about 10 km s $^{-1}$ for the radial velocities, and 0.01 for the intensity.

A few examples of our spectra are plotted in Fig.1. The long-term variability of EW and ΔV are presented in Fig.2.

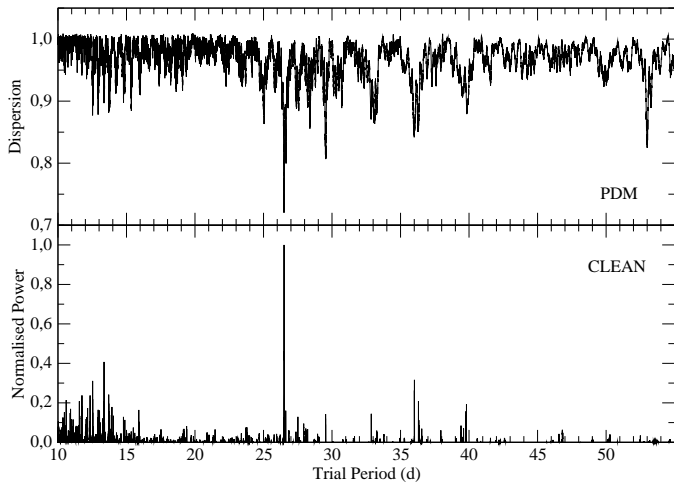


Fig. 3. Periodograms for the ratio EW_B/EW_R of LSI+61⁰303. They are computed using the PDM and CLEAN methods. The orbital period is detected in both cases as the most significant one.

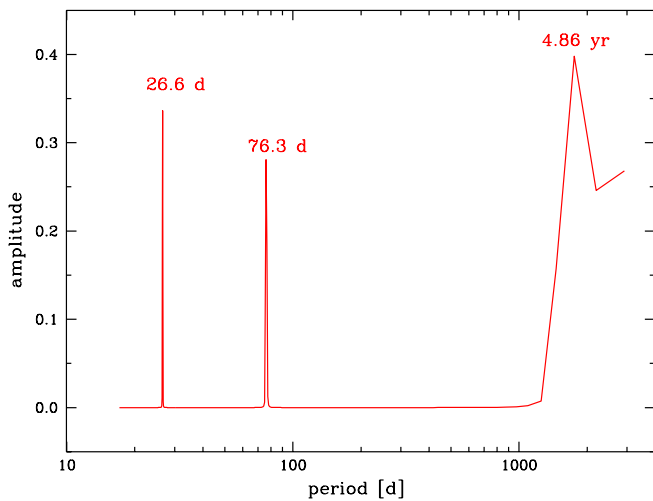


Fig. 4. Results of harmonic fit to the EW data, which clearly show the orbital period and a 4.5 yr long-term modulation.

3. Periodogram analysis of the H α parameters

3.1. Detection of the orbital variability

We conducted a period analysis for the different H α line parameters listed in Table 1, and also using data from McSwain et al. (2010), Grundstrom et al. (2007a), Liu & Yan (2005), Zamanov et al. (1999), Paredes et al. (1994), Steele et al. (1996). The period-search methods were the phase dispersion minimization (PDM) (Stellingwerf 1978) and the CLEAN algorithm (Roberts, Lehar & Dreher 1987). As a result, we confirm with a higher precision that the H α emission in LSI+61 303 displays variations with the orbital period. The orbital modulation is better revealed in the ratio $EW(B)/EW(R)$, $EW(B)$, and $V_r(cd)$.

In Fig.3 we present the PDM and CLEAN periodograms for $EW(B)/EW(R)$. The most significant period detected in the range 10 – 60 d corresponds to 26.498 d and 26.499 d for the PDM and CLEAN methods respectively. Using different H α parameters, we obtain, an averaged value 26.502 ± 0.007 d, which is not an improvement over the radio orbital period. Thus, the

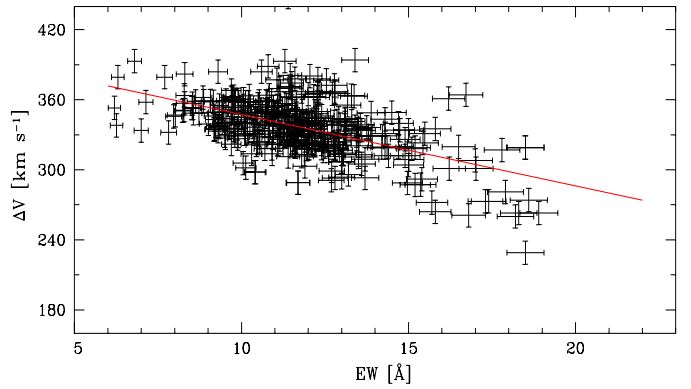


Fig. 5. ΔV versus EW (upper panel) and R_{disk} vs. EW (lower panel). The solid line is the best linear fit (see Eq.4).

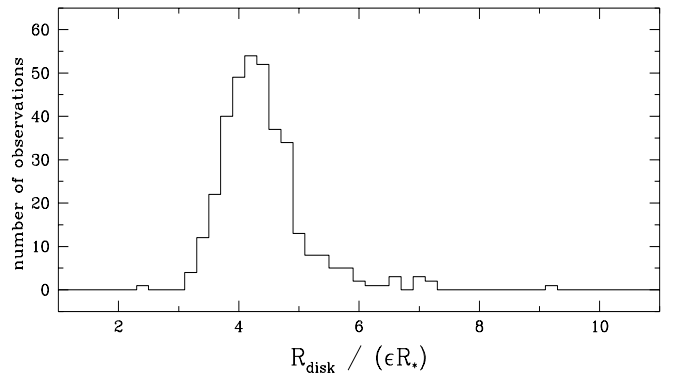


Fig. 6. Histogram of R_{disk} values. The peak of the distribution corresponds to $R_{disk} \approx 26 R_{\odot}$ (see Sect. 4.3).

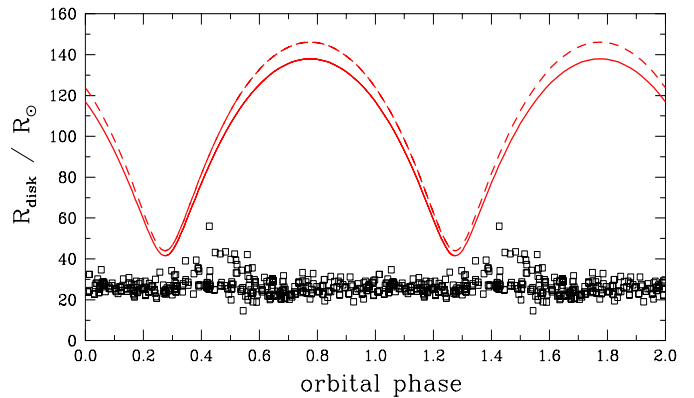


Fig. 7. Orbital variability of R_{disk} . The solid line is the distance between the components for a neutron star, the dashed line plots the distance to a black-hole companion. Interestingly, the orbital variability of R_{disk} is not in phase with the distance between the Be star and the compact object.

H α emission line appears to match the same orbital period of 26.4960 ± 0.0028 d obtained with Bayesian analysis of radio data (Gregory 2002).

3.2. Long-term variability

In addition to the orbital periodicity, another clock is operating in LSI+61⁰303, whose physical mechanism is not yet clear. The phase and amplitude of the radio outbursts are known to exhibit

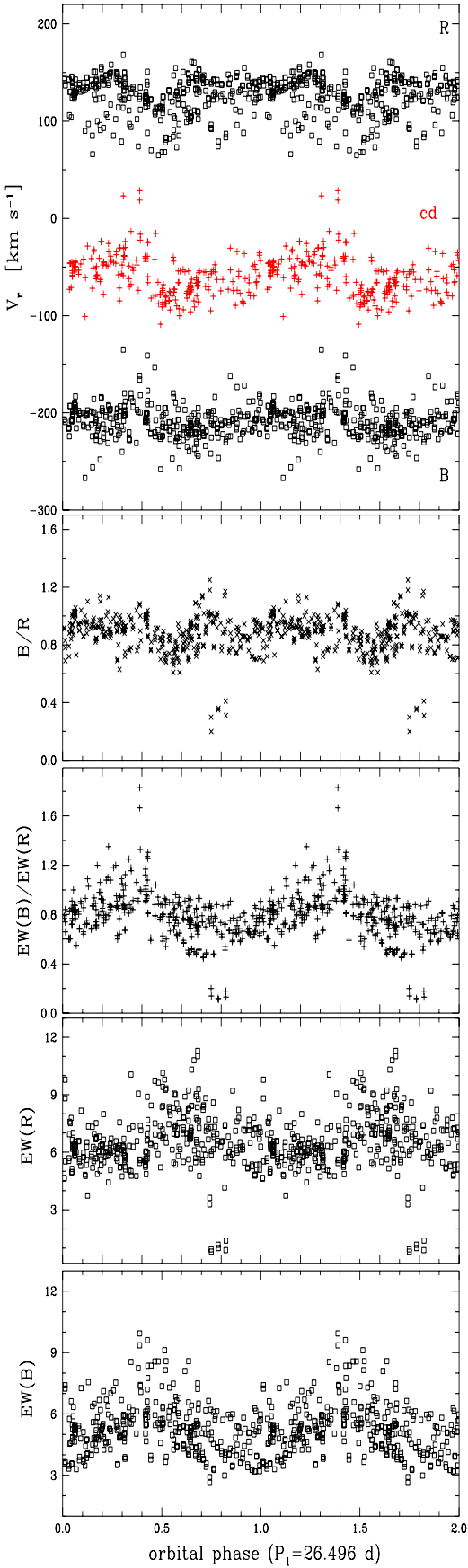


Fig. 8. $H\alpha$ parameters folded with orbital period. The following parameters are plotted (from up to down): radial velocity of the blue peak, radial velocity of the red peak, B/R ratio, the ratio of the equivalent widths of the blue and red peak, the equivalent width of the red peak, and the equivalent width of the blue peak. The radial velocities are those after JD2448868.

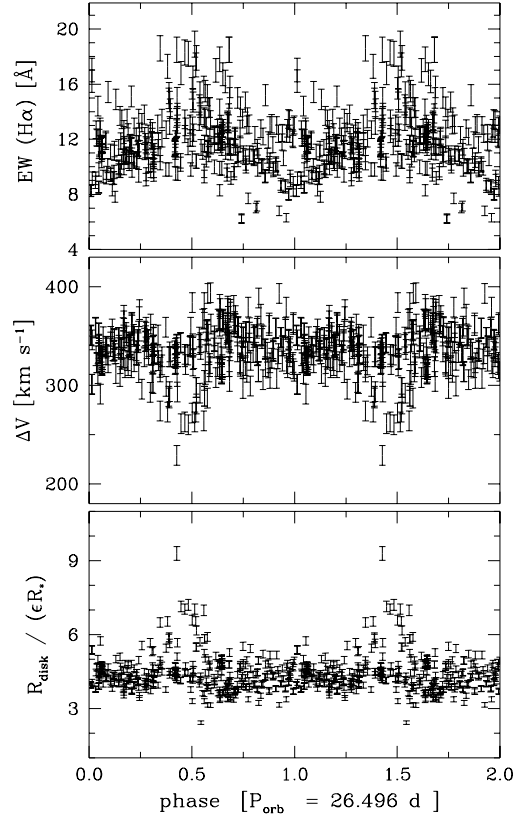


Fig. 9. EW, ΔV , and R_{disk} folded with a period of 26.496 d.

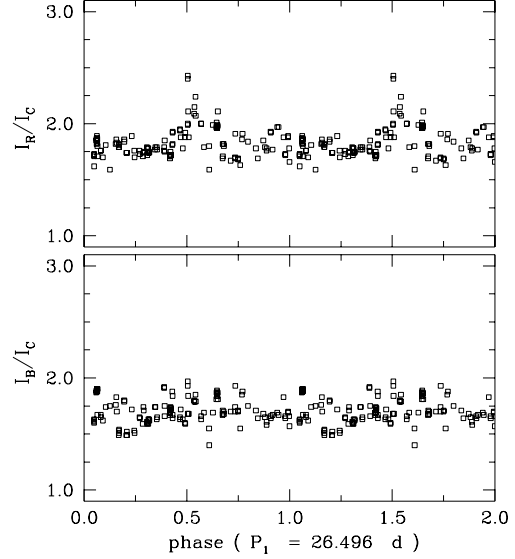


Fig. 10. Intensity of the red and blue peak of $H\alpha$ folded with orbital period. The orbital modulation is visible in I_R . These values are measured on our new spectra.

a long-term 1600-day modulation (Paredes 1987; Gregory et al. 1989; Gregory 2002).

A visual inspection of Fig.2 data suggests that a modulation of a few years may also be present. To quantitatively address this superorbital-period question, all the PDM and CLEAN analyses were extended up to 4000 d (i.e. half the full time-span of the

data). The resulting periodograms (not shown here) suggested possible frequency components around ~ 1800 d. However, a precise determination of these long-term periodicities was difficult due to the uneven sampling of the data and because only four superorbital cycles are covered. To obtain our best estimate, we applied a parametric harmonic modeling of the signal. This can be achieved in a three-stage procedure. After detrending the data, the well-known Lomb-Scargle Fourier method was applied to estimate the frequencies and number of components above the 99% confidence level. Amplitudes and phases were then determined by means of a linear fit. The resulting parameters were used as starting estimates for a nonlinear optimization. After building the component model, it was used to determine the definitive frequencies by means of traditional Fourier analysis because now the model could be evenly sampled. As a final result, we obtained a refined estimate of the initially selected frequency components.

In our case, we maintained the three main frequencies resulting from the Lomb-Scargle algorithm. Residuals are within the 90% critical limit, thus indicating that they follow a Gaussian distribution, and therefore the model seems to be well-established. Our best parametric harmonic modeling results are presented in the periodogram of Fig. 4. Here, the three main frequencies are clearly detected finally above the 99.9% confidence level. They correspond to periods of 26.6, 76.3, and 1775 d. The first value is obviously the orbital period, while the second one is close to, but not exactly coincident with, a harmonic of the former. The third period revealed in Fig.4 corresponds to a 4.86 yr modulation, that is, very similar to the period originally discovered at radio wavelengths.

This is the first time that the LSI+61 303 superorbital period is blindly detected in the optical spectroscopic properties of the source using periodogram techniques and thus confirms our early findings (Zamanov et al. 1999) that H α is modulated with a superorbital period.

4. Variability of the H α parameters

4.1. EW(H α)

In our observations, the EW(H α) of LSI+61⁰303 varies in the interval 7.8 - 18.9 Å, with average $\overline{EW} = 12.7$ Å, and standard deviation of the mean $\sigma(EW) = 2.1$ Å.

For the BeXRBs a correlation has been established between the orbital period and the maximal EW (Reig, Fabregat & Coe 1997). An updated version of this correlation is given by Reig (2011). The maximum EW of LSI+61⁰303 observed until now (EW=18.9 Å at JD 2450322) is slightly higher than the average behavior of the Be/X-ray binaries.

The linear regression for the γ -ray binaries (see Eq.2 of Casares et al. 2012a) predicts for LSI+61⁰303 a value for the maximum EW ≈ 15.5 Å. The observed value is again slightly higher than the predicted from the correlation.

4.2. BOV primary star

For the primary we assumed a B0V star of $M_1 = 12.5 \pm 2.5 M_\odot$ (Hutchings & Crampton 1981; Casares et al. 2005). We also adopted $P_{orb} = 26.496$ d and an eccentricity $e = 0.537$ (Aragona et al. 2009). For the mass of the compact object, we assumed 1.4 M_\odot for a neutron star and 4 M_\odot for a black hole (see also Aragona et al. 2009). Using Kepler's law $4\pi a^3 = G(M_1 + M_2)P_{orb}^2$, we calculated the semimajor axis of the system.

For the radius of the primary, using $M_1 = 12.5 M_\odot$ and Demircan & Kahraman (1991) equations, we obtained $R_1 = 4.3 R_\odot$ for ZAMS, $R_1 = 13.1 R_\odot$ for TAMS. The lifetime on the main sequence of a 12.5 M_\odot star is $\sim 1.8 \times 10^7$ yr. On the other hand, the cluster IC 1805 (where LSI+61⁰303 is probably born) is young. Its age is estimated to be ~ 3 Myr (Massey, Johnson & DeGioia-Eastwood 1995; Sung & Lee 1995). This means that R_1 is expected to be closer to the ZAMS than to the TAMS value. For the radius of the primary, Grundstrom et al. (2007) adopted $R_1 = 6.7 \pm 0.9 R_\odot$ from the spectral classification and Harmanec (1988) tables. This agrees with the above, and we adopted the same value.

Hanuschik (1989) gives the relation

$$\log[FWHM(H\alpha)/(1.23 v \sin i + 70)] = -0.08 \log EW + 0.14, \quad (1)$$

where FWHM and $v \sin i$ are measured in km s^{-1} , EW is in [Å] (see also Reid & Parker 2012). Using the spectra with higher S/N ($S/N \geq 60$), we measured a FWHM(H α) in the range 12.1 - 13.2 Å, and estimated $v \sin i = 349 \pm 6 \text{ km s}^{-1}$. This agrees with the previous measurement $v \sin i = 360 \text{ km s}^{-1}$ by Hutchings & Crampton (1981).

4.3. Disk size

For rotationally dominated profiles the peak separation can be regarded as a measure of the outer radius of the H α emitting disk (Huang, 1972),

$$\left(\frac{\Delta V}{2 v \sin i} \right) = \left(\frac{R_{disk}}{R_*} \right)^{-j}, \quad (2)$$

with $j = 0.5$ for Keplerian rotation and $j = 1$ for the conservation of angular momentum. We adopted $j = 0.5$, because the kinematic evidence for Be stars points to a velocity field dominated by Keplerian rotation, with little or no radial flow (Hummel & Vrancken 2000; Hanuschik 2000; Porter & Rivinius 2003 and references therein). Eq.2 relies on the assumptions that (1) the Be star is rotating critically, and (2) that the line profile shape is dominated by kinematics, and radiative transfer does not play a role. The current view is that the Be stars rotate at values of 70% - 80% of the critical rate (Porter 1996; Chauville et al. 2001). Hummel & Dachs (1992) showed that at higher optical depths the emission line peaks are shifted toward lower velocities, which means smaller peak separations. Hanuschik, Kozok & Kaiser (1988) showed that the peak separation of H α line is smaller than the peak separation of the H β line, and is probably smaller than the true kinematic value. Bearing in mind these effects, we used to calculate the disk radius

$$R_{disk} = \epsilon R_* \frac{(2v \sin i)^2}{\Delta V^2}, \quad (3)$$

where ϵ is a dimensionless parameter, for which we adopted $\epsilon = 0.9 \pm 0.1$.

Fig.2 shows the long-term variability of the EW(H α), the distance between the red and blue peaks (ΔV), and the size of the H α -emitting disk (R_{disk}). ΔV was calculated as $\Delta V = V_r(R) - V_r(B)$, and the disk size R_d was calculated from Eq.2.

In our observations ΔV varies in the interval 137 - 394 km s^{-1} , with $\overline{\Delta V} = 329 \text{ km s}^{-1}$, and $\sigma(\Delta V) = 30 \text{ km s}^{-1}$. This, following Eq.3, and assuming $\epsilon = 0.9$, $R_* = 6.7$, corresponds to R_{disk} in the interval 15 - 56 R_\odot , 90% of the calculated values are in the interval 21 - 34 R_\odot , with mean $\overline{R}_{disk} = 26.5 R_\odot$, median $< R_{disk} > = 25.8 R_\odot$, and $\sigma(R_{disk}) = 4.4 R_\odot$.

4.4. ΔV versus EW

In Fig.5 we plot ΔV versus the EW. The linear fit (of type $y = a + bx$) to the data points in Fig.5 (upper panel) gives

$$\Delta V [\text{km s}^{-1}] = 408.3(\pm 6.0) - 6.11(\pm 0.50) EW [\text{\AA}], \quad (4)$$

The errors of the coefficients are given in brackets. The Spearman (ρ) rank correlation gives $\rho = -0.47$ (significance 10^{-9}). The significance is $\ll 0.001$, indicating that the correlation is highly significant. Eq.4 was obtained on the base of 351 data pairs obtained during the past 21 years. This correlation is much shallower when we use only the new data (Table 1), probably reflecting the fact that during the time of our new observations, the 4 yr modulation is obscured.

The negative correlation between ΔV and $EW(H\alpha)$ expresses that the outer radius grows with increasing $EW(H\alpha)$ (e.g. Hanuschik, Kozok, & Kaiser, 1988). A similar behavior is also visible in the $H\alpha$ observations of the Be/X-ray binaries LS V+44 17 (Reig et al. 2005) and 4U 2206 + 54 (Blay et al. 2006).

4.5. Disk truncation

Haigh, Coe & Fabregat (2004) and Coe et al. (2006) argued that the tendency for the disk emission fluxes to cluster at specified levels is related to the presence of resonances between the disk gas and neutron star orbital periods that tend to truncate the disk at specific disk radii (Okazaki & Negueruela 2001). These truncation radii are given (see also Grundstrom et al. 2007b) by

$$R_n^{3/2} = \frac{(G M_1)^{1/2} P_{orb}}{2\pi n}, \quad (5)$$

where G is the gravitational constant and n is the integer number of disk gas rotational periods per one orbital period. The important resonances are not only those with $n : 1$, but can as well be $n : m$ in general, e.g. the 3:2 could be quite strong.

Okazaki & Negueruela (2001) found that these limiting radii are defined by the closest approach of the companion in the high-eccentricity systems and by resonances between the orbital period and the disk gas rotational periods in the low-eccentricity systems. LSI+61°303 has an orbital eccentricity that falls between these two cases, where the important resonance radii are similar in size to the periastron separation.

We calculated for LSI+61°303 the resonance radii as $R_8 = 21.7 R_\odot$, $R_7 = 23.8 R_\odot$, $R_6 = 26.3 R_\odot$, $R_5 = 29.7 R_\odot$, $R_4 = 34.5 R_\odot$, and $R_3 = 41.8 R_\odot$. The peak of the histogram (Fig.6) corresponds to $R_{disk} \approx 26 R_\odot$, which corresponds to a 6:1 resonance. Bearing in mind the uncertainty of the adopted parameters, this peak is probably in the range $R_8 \leq R_{disk} \leq R_4$.

The distance between the components at periastron is about $r(per) \approx 42 R_\odot$ for $M_2 = 1.4 M_\odot$ [$r(per) \approx 44 R_\odot$ for $M_2 = 4 M_\odot$]. Using the Eggleton (1983) formula, we calculated a Roche lobe radius $r_{RL} = 0.57$ in units of the orbital separation for $M_2 = 1.4 M_\odot$ and $r_{RL} = 0.48$ for $M_2 = 4 M_\odot$, respectively. This gives for a neutron star $r_{RL}(per) = 24 R_\odot$ and $r_{RL}(per) = 78 R_\odot$ for the periastron and apastron, respectively [for a black hole these values are $r_{RL}(per) = 21 R_\odot$ and $r_{RL}(per) = 70 R_\odot$]. For the circumstellar disk, it gives $r_{RL}(per) \approx R_{disk} < r(per) < r_{RL}(ap)$.

For a similar system 4U 0115+63 ($P_{orb} = 24.3$ d and $e = 0.34$), the numerical simulations of Okazaki et al. (2002) demonstraed that the surface density profile has breaks near the 5:1 resonance radius.

For the well-known X-ray pulsar 1A 0535+262 (HDE 245770, V725 Tau), Grundstrom et al. (2007b) confirmed the expectations for resonance disk truncation. They found that the largest disk radius is similar to both the $n=5$ resonance radius and the mean Roche lobe radius at the time of periastron. The historical maxima of $H\alpha$ strength may imply that the disk radius can occasionally grow to even larger dimensions.

For LSI+61°303 the situation is similar. The average disk size is similar to both the $n = 6 \pm 1$ resonance radius and the mean Roche lobe radius at the time of periastron. At times, it also grows to higher values.

4.6. Orbital variability of the $H\alpha$ emission line

The best estimate of the orbital period of LSI+61°303 is $P_{orb} = 26.4960 \pm 0.0028$ days derived from Bayesian analysis of the radio observations (Gregory 2002). The zero phase is by convention $JD_0 = 2,443,366.775$, the date of the first radio detection of the star (Gregory & Taylor 1978). Using this ephemeris, we plot the orbital variability of different $H\alpha$ parameters in Fig. 8, Fig 10 and 9.

According to the most recent radial velocity measurements, the orbit is elliptical ($e = 0.537 \pm 0.034$), and the periastron passage is determined to occur around phase $\phi = 0.275$, the apastron passage at $\phi = 0.775$, the superior conjunction at $\phi = 0.081$ (NS behind the BOV) and inferior conjunction (the NS passes in front of the BOV star) at $\phi = 0.313$ (Aragona et al. 2009). The eccentricity and relatively short orbital period provide significant changes in physical conditions along the orbit.

The orbital modulation is better visible in the ratio $EW(B)/EW(R)$, $EW(B)$ and $V_r(cd)$. The highest-values $EW(B)/EW(R) > 1.0$ are reached in the orbital phase interval 0.13-0.43 when the neutron star is on the left side (relatively to the line of sight) and moves toward the observer. The highest values of the $EW(B)$ are reached in the phase interval 0.3 - 0.6, the highest values of the total $EW(H\alpha)$ are also reached in the phase interval 0.3 - 0.6, where the minimum of ΔV and the maximum of R_{disk} occur as well.

The peak radio emission in each orbit occurs somewhere in range of phases extending from 0.4 to 0.9 (Gregory 2002). The onset of the outburst is $\sim 0.1 - 0.15$ earlier (Zamanov & Martí 2000). This means that the maxima of $EW(H\alpha)$ and $EW(B)$ occur more or less at the time of the start of the radio outbursts.

One might expect that the disk size varies in phase with the distance between the Be star and the compact object. However, this is not the case in LSI+61°303. R_{disk} is not in phase with the distance between the Be star and the compact object. The peak of the disk size occurs in the interval 0.3-0.6, that is, it precedes the apastron, which occurs at $\phi = 0.775$ (see Fig.7 and Fig. 9). This could be due to size variation and/or some tidal noncircular motion in the disk (e.g. Fig. 1 of Romero et al. 2007).

5. Discussion

The circumstellar disks of the Be stars are inherently time variable and can develop and disappear on timescales of years to decades (Underhill & Doazan 1982; Hubert & Floquet 1998). Disk-loss episodes has been observed in the BeXRBs X Per (Roche et al. 1997) and 1A 0535+262 (Haigh et al. 2000). For LSI+61°303 there are $H\alpha$ observations for more then 20 yr, during which period no disk-loss episode has been observed. The existence of $H\alpha$ in emission throughout the past 24 years suggests that there is a permanent gas disk around the Be star.

5.1. Orbital modulation of the EW(H α) in Be/ γ -ray binaries

Tarasov, Brocksopp & Lyuty (2003) demonstrated that the H α line-profiles of the supergiant X-ray binary Cyg X-1 show a complex variability on different timescales, controlled in particular by the orbital period and the focused wind model of the mass loss.

In our observations the EW(H α) peaks at orbital phase $\phi \sim 0.4 - 0.7$ (see Fig. 9). The detailed study of the H α emission of LSI+61⁰303 throughout an entire, single orbit (McSwain et al. 2010) demonstrated that there is a well-pronounced peak in EW(H α) at orbital phases 0.5 - 0.7. Bearing in mind that the periastron passage is at $\phi = 0.275$, we conclude that the EW(H α) peaks at 0.2 - 0.4 phases past periastron.

Casares et al. (2012a) reported spectroscopic observations of the two γ -ray binaries MWC 656 (AGL J2241+4454) and MWC 148 (HESS J0632+057). For MWC 656 (B3IV primary, $P_{orb} = 60.37$ d, $e \sim 0.40$), they detected a maximum of the EW(H α) at 0.3 phases past periastron, for MWC 148 (primary B0Ve, $P_{orb} = 321$ d, $e \approx 0.83$), with the correct phasing (see Casares et al. 2012b), the maximum in the EW of the H α line occurs ~ 0.5 orbital phases past periastron.

Apparently it is a common property of the Be/ γ -ray binaries that the maximum of the EW(H α) occurs with a delay of 0.3 - 0.5 phases past periastron.

5.2. Rotation of the components

Be stars are fast rotators. They rotate at 70% - 80% of the critical rate with a rather small intrinsic width of the distribution (Porter & Rivinius 2003 and references therein). The properties of the Be binaries with detected hot evolved companions demonstrate that some fraction of Be stars were spun up through angular-momentum transfer by Roche-lobe overflow (Peters et al. 2013). This is probably also the case for most of the Be/X-ray binaries. The rotation period of the primary in LSI+61⁰303 (B0Ve star) is estimated to be $P_{rot} \sim 0.4 - 2.6$ d, which means that it has a ratio $P_{rot}/P_{orb} \sim 0.05$, one of the higher values among the Be/X-ray binaries (Stoyanov & Zamanov 2010).

The spin period of the compact object in LSI+61⁰303 is still unknown. The deep searches in the radio- (McSwain et al. 2011, Cañellas et al. 2012) and X-ray band (Rea et al. 2010) did not detect pulsed fraction so far. The ejector-propeller model of LSI+61⁰303 predicts a spin period of the neutron star of 0.15-0.20 s (Zamanov 1995; Zamanov, Marti & Marziani, 2001). One more prediction can be made using the Corbet diagram (Corbet 1986). The equation $\log P_{spin} = -1.011 + 1.447 \log P_{orb}$ (where P_{spin} is in seconds, P_{orb} is in days), which seems to be valid for wind-fed sources (X-ray pulsars in Be/X-ray binaries and white dwarfs in symbiotic stars), predicts $P_{spin} \approx 11$ s.

5.3. Shell criterion and the Be star inclination

The Be-shell stars are identified as normal Be stars viewed edge-on (Porter 1996; Rivinius, Štefl & Baade 2006). Comparing the FeII and H α line profile, Hanuschik (1996) found that the shell stars are those with $I_p/I_{cd}(H\alpha) \geq 1.5$, where I_p and I_{cd} are the mean peak intensity and the intensity of the central depression, respectively.

In our spectroscopic observations of LSI+61⁰303, $I_p/I_{cd}(H\alpha)$ varies in the range 1.16-1.70. Removing the four highest and four lowest values, we obtain a range of 1.20-1.53, a mean value of 1.40, and a standard deviation of the mean 0.08. It falls in the intermediate cases according

to Eq.3 of Hanuschik (1996). Among our 130 measurements there are about a dozen values with $I_p/I_{cd} \geq 1.5$, and the Be star of LSI+61⁰303 fulfills the shell criterion (e.g. 1998/10/04, 2012/07/07). The spectrum 20120707164 is plotted in the bottom panel of Fig.1 and it is visible that the central dip of H α intensifies and the central absorption of HeI λ 6678 deepens as well. The specific effect of the transition to the Be-shell type is expected only at about an inclination angle $i \approx 70^\circ \pm 5^\circ$ (Hanuschik 1996). This suggests that the inclination of the primary star in LSI+61⁰303 to the line of sight is probably $i \sim 70^\circ$.

One more clue for the inclination can be given using the full width at zero intensity (FWZI). For an optically thin line this is connected with the inclination, $FWZI/2 \times \sin i = (GM_1/R_1)^{1/2}$ (see Casares et al. 2012a and references therein). The FWZI of the H α line is ~ 60 Å, but it is not optically thin and other mechanisms are broadening it. The FWZI of HeI λ 6678 line is $19.0 (\pm 10\%)$ Å, which points again to a high inclination $i \sim 90^\circ$.

5.4. Connection between H α and high-energy emission

The nonthermal behavior of the source has been studied often, but is still poorly understood. The nonthermal radio emission presents a well-defined periodicity with strong flares that occur periodically near apastron passage, along with an additional modulation on a 4.6 year timescale (Gregory 2002). The detection of extended structures in radio observations originally identified LS I +61⁰ 303 as a potential microquasar, with high-energy emission produced in jets driven by accretion onto the compact object, presumably a black hole (Massi et al. 2001). However, high-resolution VLBA observations indicate that the radio structures are not persistent and can be more easily explained by the interaction between a pulsar wind and the wind of the stellar companion (Dhawan, Mioduszewski & Rupen 2006, Albert et al. 2008), although alternative interpretations are still possible (Romero et al. 2007, Massi and Zimmerman 2010). Many arguments in favor of LS I +61⁰ 303 as a nonaccreting pulsar system have been summarized by Torres et al. (2010). The high-energy process that causes the very high energy emission could also produce neutrino flux. No evidence for periodic neutrino emission is found in the IceCube Neutrino Observatory data (Abbasi et al. 2012) until now.

5.4.1. Connection between H α and γ -rays

The gamma-ray flux (> 0.1 GeV) also displays orbital modulation. Its maximum is at orbital phases 0.35 - 0.55 and the minimum at 0.9 - 1.0 (Hadasch et al. 2012). The maximum of the gamma-ray flux coincides with the maxima of the EW(H α), EW(B), and R_{disk} (see also Fig.9). The minimum of the gamma-ray flux corresponds to the minima of EW(H α) and EW(B).

A flux change in gamma rays (Hadasch et al. 2012) occurred in March 2009 (around JD 2454900). Before the transition, the modulation was clearly visible and was compatible with the previously published phasogram, whereas afterwards, the amplitude of the modulation diminished. This transition in gamma-rays corresponds to a minimum value of the EW(H α). On February 6, 2009 we observed an EW(H α)=7.8 Å, which is considerably below the average value (see also Fig.2). This is approximately the minimum of 1600-day modulation of the EW(H α).

5.4.2. Connection between H α and X-rays

Torres et al. (2010) showed that the soft-X-ray emission from LSI+61°303 presents a periodic behavior at the orbital period, with a varying shape. Profile variability is seen from orbit to orbit on a multi-year timescale. In their analysis the orbital peak of the soft X-rays (see Fig.2 of Torres et al. 2010) is at phases 0.4 - 0.7. This coincides well with the EW, EW(B) and ΔV peaks, which occur at the same orbital phases $\phi \sim 0.4 - 0.7$ (see Fig. 9).

Simultaneous X-ray and radio observations show that periodic radio flares always lag the X-ray flare by $\Delta\phi \simeq 0.2$ (Chernyakova et al. 2012), a behavior predicted by the ejector - propeller model. Additionally, intense X-ray flares have been observed (Smith et al. 2009 and Torres et al. 2010), during which the flux increased by up to a factor of five and variability on a timescale of a few seconds was observed. But because of the relatively large RXTE-PCA field-of-view ($\sim 1^\circ$ FWHM), it cannot be ruled out that these flares are caused by an unrelated source in the same field. If such flares are generated in LSI+61°303, they are probably the reason for the dramatic decline in the H α emission observed in October 1999, which may have been caused by a sudden ionization of the disk (see Grundstrom et al. 2007a).

6. Conclusions

We summarize the main results of our spectral observations of the Be/X-ray binary LSI+61°303 as follows:

1. We measured various parameters of the H α emission line - equivalent widths, radial velocities, and intensities.
2. The periodogram analysis confirmed that the H α emission is modulated with the orbital and superorbital periods. The values are practically identical to those detected in the radio observations.
3. For the past 20 years the radius of the circumstellar disk is similar to the Roche lobe radius at periastron. It is probably truncated by a resonance of $n = 6 \pm 1$.
4. The orbital maxima of the equivalent width of H α emission and the radius of the circumstellar disk peak after the periastron and coincide on average with the X-ray and γ -ray maxima.
5. For the B0V primary, we estimated a projected rotational velocity $v \sin i = 349 \pm 8 \text{ km s}^{-1}$. Its inclination to the line of sight is probably about 70° .

In future it will be interesting to compare the H α variability of LSI+61°303 in detail with the variation in X-rays and γ -rays.

Acknowledgements. We thank the anonymous referee for constructive comments. This work was supported in part by the OP "HRD", ESF and Bulgarian Ministry of Education, Youth and Science under the contract BG051PO001-3.3.06-0047. JM and PLLE acknowledge support by grant AYA2010-21782-C03-03 from the Spanish Government, and Consejería de Economía, Innovación y Ciencia of Junta de Andalucía as research group FQM-322, as well as FEDER funds.

References

Abbasi, R., Abdou, Y., Abu-Zayyad, T., et al. 2012, *ApJ*, 748, 118
Abdo, A. A., Ackermann, M., Ajello, M., et al. 2009, *ApJ*, 701, L123
Acciari, V. A., Beilicke, M., Blaylock, G., et al. 2008, *ApJ*, 679, 1427
Albert, J., Aliu, E., Anderhub, H., et al. 2006, *Science*, 312, 1771
Albert, J., Aliu, E., Anderhub, H., et al. 2008, *ApJ*, 684, 1351
Apparao, K. M. V. 2001, *A&A*, 371, 672
Aragona, C., McSwain, M. V., Grundstrom, E. D., et al. 2009, *ApJ*, 698, 514

Balona, L. A. 2000, *IAU Colloq. 175: The Be Phenomenon in Early-Type Stars*, 214, 1
Bignami, G. F., Caraveo, P. A., Lamb, R. C., Markert, T. H., & Paul, J. A. 1981, *ApJ*, 247, L85
Bildsten, L., Chakrabarty, D., Chiu, J., et al. 1997, *ApJS*, 113, 367
Blay, P., Negueruela, I., Reig, P., et al. 2006, *A&A*, 446, 1095
Cañellas, A., Joshi, B. C., Paredes, J. M., et al. 2012, *A&A*, 543, A122
Casares, J., Ribó, M., Ribas, I., et al. 2012a, *MNRAS*, 421, 1103
Casares, J., Ribó, M., Ribas, I., et al. 2012b, *MNRAS*, 426, 796
Chauville, J., Zorec, J., Ballereau, D., et al. 2001, *A&A*, 378, 861
Chernyakova, M., Neronov, A., Molkov, S., et al. 2012, *ApJ*, 747, L29
Coe, M. J., Reig, P., McBride, V. A., Galache, J. L., & Fabregat, J. 2006, *MNRAS*, 368, 447
Corbet, R. H. D. 1986, *MNRAS*, 220, 1047
Demircan, O., & Kahraman, G. 1991, *Ap&SS*, 181, 313
Dhawan, V., Mioduszewski, A., & Rupen, M. 2006, *VI Microquasar Workshop: Microquasars and Beyond*,
Eggleton, P. P. 1983, *ApJ*, 268, 368
Gregory, P. C., & Taylor, A. R. 1978, *Nature*, 272, 704
Gregory, P. C., Taylor, A. R., Crampton, D., et al. 1979, *AJ*, 84, 1030
Gregory, P. C., Xu, H.-J., Backhouse, C. J., & Reid, A. 1989, *ApJ*, 339, 1054
Gregory, P. C. 2002, *ApJ*, 575, 427
Greiner, J., & Rau, A. 2001, *A&A*, 375, 145
Grundstrom, E. D., Caballero-Nieves, S. M., Gies, D. R., et al. 2007a, *ApJ*, 666, 437
Grundstrom, E. D., Boyajian, T. S., Finch, C., et al. 2007b, *ApJ*, 660, 1398
Hadasch, D., Torres, D. F., Tanaka, T., et al. 2012, *ApJ*, 749, 54
Hanuschik, R. W., Kozok, J. R., & Kaiser, D. 1988, *A&A*, 189, 147
Hanuschik, R. W. 1989, *Ap&SS*, 161, 61
Hanuschik, R. W. 1996, *A&A*, 308, 170
Hanuschik, R. W. 2000, *IAU Colloq. 175: The Be Phenomenon in Early-Type Stars*, 214, 518
Hermesen, W., Swanenburg, B. N., Bignami, G. F., et al. 1977, *Nature*, 269, 494
Hummel, W., & Dachs, J. 1992, *A&A*, 262, L17
Haigh, N. J., Coe, M. J., Steele, I. A., & Fabregat, J. 2000, *IAU Colloq. 175: The Be Phenomenon in Early-Type Stars*, 214, 735
Haigh, N. J., Coe, M. J., & Fabregat, J. 2004, *MNRAS*, 350, 1457
Harrison, F. A., Ray, P. S., Leahy, D. A., Waltman, E. B., & Pooley, G. G. 2000, *ApJ*, 528, 454
Huang S.-S., 1972, *ApJ* 171, 549
Hubert, A. M., & Floquet, M. 1998, *A&A*, 335, 565
Hummel, W., & Vrancken, M. 2000, *A&A*, 359, 1075
Hummel, W., & Dachs, J. 1992, *A&A*, 262, L17
Hutchings, J. B., & Crampton, D. 1981, *PASP*, 93, 486
Leahy, D. A. 2001, *International Cosmic Ray Conference*, 6, 2524
Li, J., Torres, D. F., Zhang, S., et al. 2012, *ApJ*, 744, L13
Liu, Q. Z., & Yan, J. Z. 2005, *New A*, 11, 130
Massi, M., Ribó, M., Paredes, J. M., Peracaula, M., & Estalella, R. 2001, *A&A*, 376, 217
Massi, M., Ribó, M., Paredes, J. M., et al. 2004, *A&A*, 414, L1
Massi, M., & Zimmermann, L. 2010, *A&A*, 515, A82
Massi, M., Ros, E., & Zimmermann, L. 2012, *A&A*, 540, A142
McSwain, M. V., Grundstrom, E. D., Gies, D. R., & Ray, P. S. 2010, *ApJ*, 724, 379
McSwain, M. V., Ray, P. S., Ransom, S. M., et al. 2011, *ApJ*, 738, 105
Mendelson, H., & Mazeh, T. 1994, *MNRAS*, 267, 1
Mirabel, I. F., Rodrigues, I., & Liu, Q. Z. 2004, *A&A*, 422, L29
Okazaki, A. T., & Negueruela, I. 2001, *A&A*, 377, 161
Paredes, J. M., Martí, J., Peracaula, M., & Ribó, M. 1997, *A&A*, 320, L25
Paredes, J. M., 1987, PhD Thesis, Universitat de Barcelona
Paredes, J. M., Marziani, P., Martí, J., et al. 1994, *A&A*, 288, 519
Paredes, J. M., Bednarek, W., Bordas, P., et al. 2013, *Aph*, 43, 4301
Peters, G. J., Pewett, T. D., Gies, D. R., Touhami, Y. N., & Grundstrom, E. D. 2013, *ApJ*, 765, 2
Porter, J. M. 1996, *MNRAS*, 280, L31
Porter, J. M., & Rivinius, T. 2003, *PASP*, 115, 1153
Punsly, B. 1999, *ApJ*, 519, 336
Rea, N., Torres, D. F., van der Klis, M., et al. 2010, *MNRAS*, 405, 2206
Reid, W. A., & Parker, Q. A. 2012, *MNRAS*, 425, 355
Reig, P., Fabregat, J., & Coe, M. J. 1997, *A&A*, 322, 193
Reig, P., Negueruela, I., Fabregat, J., Chato, R., & Coe, M. J. 2005, *A&A*, 440, 1079
Reig, P. 2011, *Ap&SS*, 332, 1
Rivinius, T., Stefl, S., & Baade, D. 2006, *A&A*, 459, 137
Roberts, D. H., Lehar, J., & Dreher, J. W. 1987, *AJ*, 93, 968
Roche, P., Larionov, V., Tarasov, A. E., et al. 1997, *A&A*, 322, 139
Romero, G. E., Okazaki, A. T., Orellana, M., & Owocki, S. P. 2007, *A&A*, 474, 15
Slettebak, A. 1988, *PASP*, 100, 770
Smith, A., Kaaret, P., Holder, J., et al. 2009, *ApJ*, 693, 1621
Steele, I. A., Coe, M. J., Fabregat, J., et al. 1996, *A&AS*, 120, 213
Stellingwerf, R. F. 1978, *ApJ*, 224, 953
Stoyanov, K. A., & Zamanov, R. K. 2009, *Astronomische Nachrichten*, 330, 727
Sung, H., & Lee, S.-W. 1995, *Journal of Korean Astronomical Society*, 28, 119
Tarasov, A. E., Brocksopp, C., & Lyuty, V. M. 2003, *A&A*, 402, 237
Taylor, A. R., Kenny, H. T., Spencer, R. E., & Tzioumis, A. 1992, *ApJ*, 395, 268
Torres, D. F., Zhang, S., Li, J., et al. 2010, *ApJ*, 719, L104
Underhill, A., & Doazan, V. 1982, *B Stars with and without emission lines (NASA SP-456)*
Zaitseva, G. V., & Borisov, G. V. 2003, *Astronomy Letters*, 29, 188
Zamanov, R. K. 1995, *MNRAS*, 272, 308
Zamanov, R., & Martí, J. 2000a, *A&A*, 358, L55
Zamanov, R. K., Martí, J., Paredes, J. M., et al. 1999, *A&A*, 351, 543
Zamanov, R., Martí, J., & Marziani, P. 2001, *The Second National Conference on Astrophysics of Compact Objects*, 50 (astro-ph/0110114)

Table 1. H α observations of LSI+61⁰303.

spectrum ID yyyymmdd..	JD -start	exp min	S/N	EW Å	$V_r(R)$ km s ⁻¹	$V_r(B)$ km s ⁻¹	$V_r(cd)$ km s ⁻¹	EW(B/R)	I_B	I_R	I_{cd}	$V_r\text{HeI}$ km s ⁻¹
1998093003	51087.4054	20	47	14.97	122.9	-165.9	18.7	1.666	1.92	1.79	1.49	—
1998093004	51087.4196	20	45	15.36	125.5	-161.8	28.3	1.828	1.91	1.76	1.47	—
1998100157	51088.4664	20	57	15.01	121.1	-187.7	-24.0	1.255	1.88	1.81	1.39	-2.9
1998100158	51088.4922	20	51	13.70	115.9	-177.2	-25.0	1.305	1.84	1.82	1.38	-21.2
1998100159	51087.5063	20	56	13.00	111.7	-181.9	-22.5	1.327	1.75	1.75	1.38	-19.8
1998100417	51091.3185	20	37	13.30	131.7	-209.8	-85.3	0.782	1.80	2.09	1.29	-67.9
1998100418	51091.3327	20	40	14.50	131.1	-217.9	-84.4	0.734	1.79	2.15	1.32	-64.9
1998100438	51091.4910	20	44	14.30	124.6	-218.7	-76.1	0.803	1.79	2.07	1.27	-60.9
1998100439	51090.5051	20	52	14.70	125.2	-214.7	-74.4	0.749	1.84	2.11	1.29	-68.6
1998100970	51096.5846	20	50	11.66	123.6	-199.2	-73.6	0.750	1.70	1.70	1.26	-47.7
1998100971	51096.5988	20	46	12.75	122.9	-198.7	-70.2	0.766	1.74	1.69	1.27	-45.5
1998120914	51156.5455	20	21	13.03	124.7	-189.5	-43.4	0.847	1.66	1.78	1.29	—
1998120915	51156.5596	20	14	12.00	—	—	—	0.908	1.57	1.66	—	—
1999010512	51184.3724	20	30	12.12	139.7	-201.1	-56.1	0.824	1.62	1.72	1.21	-44.2
1999010513	51184.3870	20	37	11.15	138.9	-198.6	-58.6	0.768	1.63	1.73	1.19	-34.9
1999010515	51184.4014	20	37	11.28	139.5	-202.2	-59.6	0.753	1.60	1.71	1.21	-48.7
1999010600	51185.2539	20	42	11.86	133.1	-198.0	-53.4	0.802	1.67	1.76	1.17	-31.9
1999010699	51185.2398	20	53	12.00	132.3	-206.9	-57.5	0.825	1.65	1.76	1.18	-38.9
1999030671	51244.2408	20	44	12.18	131.4	-208.2	-42.5	0.950	1.60	1.75	1.26	-36.6
1999030672	51244.2549	20	31	11.84	136.1	-203.1	-31.0	0.870	1.59	1.72	1.29	-20.3
1999030673	51244.2692	20	42	12.58	123.1	-198.3	-38.4	0.878	1.60	1.78	1.28	-35.4
1999032619	51264.2936	20	42	11.59	142.9	-183.1	-49.5	0.766	1.67	1.71	1.19	-27.8
1999091752	51439.4167	20	48	13.18	144.1	-211.3	-63.4	0.695	1.68	1.82	1.20	-46.8
1999091771	51439.5593	20	52	13.88	141.1	-207.7	-69.8	0.663	1.70	1.82	1.18	-53.0
1999091772	51439.5735	20	57	13.11	133.2	-210.6	-66.1	0.710	1.68	1.80	1.18	-48.9
1999091937	51441.4296	20	46	10.98	138.4	-210.9	-57.0	0.868	1.71	1.68	1.17	-32.9
1999091938	51441.4437	20	45	10.80	140.0	-208.5	-54.8	0.784	1.70	1.69	1.21	-38.2
2000012713	51571.2966	20	67	16.72	160.9	-203.3	-62.5	0.622	1.81	2.11	1.28	-66.9
2000062161	51717.4849	5	23	12.72	141.7	-223.5	-62.0	0.693	1.53	1.81	1.14	-9.6
2000062162	51717.4943	20	41	11.46	143.4	-227.8	-60.3	0.709	1.49	1.79	1.14	-2.7
2000062163	51717.5091	20	40	9.91	134.1	-223.8	-58.8	0.743	1.54	1.82	1.13	-5.6
2000062164	51717.5241	20	53	11.63	140.9	-207.3	-49.7	0.717	1.51	1.79	1.14	-28.5
2000062387	51718.4960	20	40	11.52	141.4	-221.2	-45.8	0.731	1.49	1.74	1.19	-11.5
2000062388	51718.5107	20	56	10.83	137.5	-226.4	-44.8	0.793	1.49	1.74	1.13	-29.3
2000062389	51718.5252	20	45	9.73	145.0	-216.0	—	0.775	1.52	1.74	1.13	-43.1
2000062393	51719.4816	20	40	11.15	150.0	-219.8	-42.6	0.864	1.53	1.76	1.19	-7.3
2000062395	51719.5108	20	31	12.54	157.9	-218.9	-44.2	0.869	1.51	1.70	1.19	—
2000081776	51774.3832	16	36	11.15	143.5	-188.5	-23.8	1.124	1.63	1.75	1.21	-8.0
2000081777	51774.3956	20	48	10.37	135.6	-197.3	-30.0	1.035	1.62	1.74	1.23	-5.2
2000081819	51775.3947	20	41	13.51	132.5	-188.1	-50.4	0.840	1.63	1.79	1.34	-10.2
2000081820	51775.4073	15	44	12.03	135.1	-194.0	-53.5	0.914	1.65	1.77	1.30	-35.5
2000081985	51776.3989	20	55	14.74	134.5	-199.5	-16.4	1.000	1.66	1.85	1.29	-31.9
2000082038	51777.3920	20	53	13.91	120.9	-207.9	-59.9	0.811	1.64	1.92	1.28	-67.8
2000082039	51777.4082	20	68	13.10	118.4	-214.7	-66.1	0.808	1.67	1.93	1.29	-48.1
2000082105	51778.3539	20	50	13.45	109.0	-220.1	-78.6	0.792	1.63	1.95	1.30	-54.9
2000082106	51778.3681	20	52	12.38	107.2	-224.2	-80.2	0.788	1.65	1.94	1.30	-53.3
2000082206	51779.3545	20	46	12.09	118.7	-223.5	-72.1	0.786	1.68	2.00	1.26	-44.6
2000082207	51779.3687	20	48	12.96	114.2	-224.5	-76.1	0.800	1.68	1.99	1.29	-37.6
2000091723	51805.5042	20	61	12.10	115.0	-224.6	-78.0	0.763	1.60	1.88	1.27	-71.0
2000091724	51805.5261	20	64	13.10	113.5	-226.8	-77.9	0.777	1.59	1.92	1.29	-58.4
2000120547	51884.4345	20	67	12.90	113.7	-207.5	-15.5	1.040	1.72	1.88	1.45	-56.3
2000120669	51885.4853	20	65	12.48	124.8	-202.2	-68.2	0.803	1.68	1.88	1.37	-49.8
20001208200	51887.4365	20	68	10.92	117.1	-196.5	-54.0	0.882	1.69	1.79	1.22	-49.5
20010204161	51945.3274	20	49	13.05	129.6	-183.7	-47.7	0.785	1.85	1.86	1.33	-13.0
20010206208	51947.4100	20	65	10.05	143.7	-162.1	-30.6	0.752	1.64	1.69	1.22	-50.0
20010207226	51948.2957	20	61	10.48	149.5	-173.5	-34.2	0.753	1.65	1.79	1.18	-28.1

Table 1. Continued.

20010208261	51949.2902	20	71	9.89	154.8	-171.9	-36.3	0.811	1.67	1.77	1.13	-16.4
20010317356	51986.2288	20	51	10.13	121.7	-180.0	-39.3	0.851	1.63	1.78	1.15	-38.4
20010317357	51986.2458	20	42	10.53	131.3	-193.0	-38.2	0.843	1.59	1.74	1.18	-34.0
2001040730	52007.2424	20	40	11.09	139.4	-199.8	-41.8	0.855	1.74	1.81	1.19	-33.8
2001070958	52100.5735	20	53	11.79	107.7	-225.2	-82.1	0.826	1.69	1.99	1.28	-58.5
2001072790	52118.5316	20	43	11.97	113.8	-217.0	-59.0	0.890	1.61	1.79	1.23	-56.0
20010903161	52156.4462	20	44	14.36	117.3	-202.1	-61.0	0.860	1.93	1.91	1.31	-50.3
20010904214	52157.3702	20	50	13.60	127.7	-206.2	-55.1	0.770	1.88	1.91	1.28	-59.1
2001100323	52186.5529	20	61	11.95	111.6	-206.1	-89.5	0.679	1.68	1.85	1.28	-83.5
2002012348	52298.3445	20	65	10.09	130.3	-200.5	-47.0	0.908	1.62	1.70	1.21	-52.9
2002062229	52448.5433	20	44	10.69	126.0	-212.6	-80.1	0.738	1.55	1.63	1.19	-29.1
2002062418	52450.5460	20	39	12.78	147.9	-224.4	-73.0	0.876	1.71	1.78	1.17	-26.5
2002102031	52568.4718	20	58	11.20	143.3	-203.2	-71.7	0.766	1.59	1.71	1.25	-6.4
2002111224	52591.4611	20	58	11.87	137.9	-199.8	-51.0	0.892	1.76	1.82	1.28	-18.0
2003071728	52838.5832	20	65	11.46	112.8	-217.8	-65.8	0.942	1.63	1.78	1.29	-63.7
20031205111	52979.461	20	73	10.95	125.7	-207.6	-74.5	0.735	1.75	1.84	1.21	-48.7
20031208143	52982.393	20	34	10.12	136.7	-221.4	-85.2	0.606	1.66	1.93	1.23	-59.3
20031208144	52982.408	20	38	10.21	136.4	-221.3	-86.6	0.664	1.64	1.92	1.18	-57.0
20031209181	52983.399	20	43	10.62	128.8	-211.3	-79.6	0.638	1.67	1.97	1.22	-72.1
20041001	53280.5038	20	55	13.45	127.1	-199.2	-32.4	0.935	1.70	1.83	1.20	-33.5
20060116	53752.4002	19	33	13.47	119.4	-215.4	-47.5	0.871	1.83	1.88	1.31	—
20061202	54072.4667	20	28	11.43	136.6	-198.7	-53.8	0.849	1.61	1.62	1.15	—
2007040116	54192.2496	20	19	15.84	—	—	—	0.760	1.63	2.00	1.18	—
20070401	54192.2496	20	19	12.91	154.6	-189.4	—	0.752	1.66	2.00	1.28	—
2007040232	54193.2420	20	31	12.36	150.4	-187.6	-52.4	0.772	1.55	1.80	1.20	—
2007040236	54193.2700	20	15	12.58	—	—	—	0.760	1.40	1.59	1.11	—
2008012541	54491.4239	20	31	9.64	—	-206.2	-74.2	0.772	—	—	1.07	-74.1
2008032959	54555.2378	20	39	12.23	143.9	-204.1	-37.4	0.860	1.65	1.76	1.27	—
2008032965	54555.2603	20	47	11.08	150.3	-204.6	-34.5	0.952	1.64	1.73	1.28	—
2009011162a	54843.3744	20	39	10.00	142.3	-198.4	-41.2	—	—	—	1.25	-45.2
20090206104	54869.3824	20	30	7.82	134.6	-197.4	-28.5	1.090	1.75	1.59	0.95	-27.2
2010102374	55493.3172	20	57	12.29	148.2	-229.7	-66.9	0.850	1.67	1.69	1.24	—
2010102377	55493.3374	20	76	12.05	148.6	-231.7	-61.3	0.845	1.71	1.71	1.26	-45.9
20101024129	55494.3266	20	57	11.41	147.0	-223.8	-55.1	0.859	1.70	1.67	1.27	-17.5
2010112406	55525.4759	4	13	13.56	—	—	-59.5	0.652	1.61	1.76	1.23	—
2010112407	55525.4847	20	35	13.13	129.9	-197.7	-54.5	0.686	1.58	1.78	1.16	—
2010122228	55553.3332	20	53	12.76	136.7	—	-66.2	0.658	0.00	0.00	1.26	—
2010122229	55553.3474	20	47	12.46	136.0	-188.5	-60.6	0.690	1.69	1.97	1.25	-55.5
2011011923	55581.2366	20	58	12.00	140.2	-182.9	-38.0	0.791	1.69	1.88	1.23	-38.3
2011011924	55581.2515	20	62	12.93	136.3	-180.6	-35.6	0.777	1.70	1.89	1.22	-34.5
20110422107	55674.2894	20	52	16.50	108.3	-211.4	-88.6	0.627	1.93	2.40	1.58	-55.4
20110422108	55674.3063	20	53	14.90	112.0	-214.1	-86.3	0.584	1.97	2.43	1.59	-68.3
20110423145	55675.2838	20	34	13.75	109.3	-227.0	-94.2	0.667	1.85	2.24	1.44	-79.5
20110905123	55810.4711	20	57	11.80	100.3	-211.4	-69.8	0.763	1.81	1.97	1.33	-39.5
20110905124	55810.4861	20	56	11.40	100.3	-211.0	-69.5	0.689	1.87	2.01	1.31	-39.9
20110905125	55810.5003	20	57	11.88	104.9	-208.3	-68.6	0.718	1.87	1.96	1.29	-36.1
20110905126	55810.5144	20	52	12.20	108.6	-212.3	-66.2	0.774	1.84	1.98	1.35	-44.6
20110905127	55810.5286	20	53	12.02	104.2	-214.4	-71.3	0.754	1.89	1.96	1.32	-49.7
20110905128	55810.5427	20	67	12.45	105.0	-211.1	-70.9	0.746	1.86	1.96	1.33	-47.3
20110905130	55810.5583	20	64	12.60	103.2	-213.0	-73.1	0.733	1.86	1.97	1.33	-42.9
20110905131	55810.5724	20	60	11.98	104.5	-213.6	-75.7	0.749	1.84	1.99	1.32	-47.6
20110905132	55810.5869	20	69	12.40	104.4	-214.1	-73.8	0.751	1.87	1.98	1.32	-56.8
20111108059	55874.4505	20	57	11.52	123.0	—	-49.6	0.875	1.87	1.85	1.35	-16.5
20111108060	55874.4661	20	55	11.60	124.9	-194.6	—	0.818	1.89	1.86	1.36	-28.8
20111108061	55874.4956	20	65	10.94	130.5	-189.5	-53.5	0.831	1.88	1.82	1.35	—
20111108062	55874.5106	20	60	10.45	126.6	-190.9	-55.1	0.801	1.89	1.87	1.37	-37.8
20111108063	55874.5279	20	56	11.63	129.7	-194.5	-45.2	0.842	1.90	1.89	1.35	-19.9
20111108064	55874.5428	20	49	11.15	128.5	-197.5	-49.2	0.894	1.89	1.85	1.38	—
20111108065	55874.5579	20	56	11.07	129.2	-192.5	-45.4	0.840	1.88	1.86	1.35	-25.4
20111108066	55874.5725	20	56	11.62	128.3	-191.9	-43.9	0.818	1.90	1.87	1.36	-27.4
20111108067	55874.5870	20	52	11.71	130.1	-198.6	-49.4	0.873	1.88	1.83	1.35	-39.2

Table 1. Continued.

20111108068	55874.6016	20	50	11.56	129.6	-196.3	-49.7	0.837	1.90	1.80	1.32	-38.1
20111214176	55910.4263	20	39	11.28	125.8	-209.2	-39.2	1.122	1.69	1.72	1.41	-11.7
20111214179	55910.4459	20	49	11.35	120.5	-207.9	-41.0	1.167	1.69	1.69	1.43	-1.6
20111214180	55910.4600	20	31	10.55	118.9	-209.3	—	0.914	1.67	1.72	1.41	-0.2
20111214181	55910.4742	20	52	11.38	123.1	-207.7	-40.7	1.006	1.69	1.71	1.46	-17.6
20111214182	55910.4883	20	50	11.47	115.2	-205.8	-39.3	0.905	1.73	1.71	1.44	-0.8
20111214183	55910.5025	20	52	12.02	129.7	-208.0	-44.2	0.989	1.74	1.75	1.44	—
20111214184	55910.5166	20	46	11.29	123.7	-205.5	—	1.032	1.71	1.72	1.43	-9.0
20111214185	55910.5308	20	33	11.10	122.6	-199.6	—	0.965	1.72	1.72	1.38	-5.0
20111214186	55910.5449	20	35	9.52	126.1	-201.1	—	0.961	1.71	1.71	1.44	-21.1
20111214187	55910.5591	20	36	11.50	123.9	-207.5	—	0.915	1.73	1.72	1.39	-20.0
20120707126	56115.5039	20	32	10.34	150.8	-185.8	-34.0	0.870	1.83	1.86	1.28	-24.9
20120707163	56116.5151	20	34	10.25	155.6	-183.8	-23.9	0.926	1.79	1.84	1.19	-2.3
20120707164	56116.5306	20	53	10.84	153.4	-184.9	-23.8	0.928	1.80	1.86	1.19	0.6
20120708046	56117.5046	20	49	10.50	137.1	-193.3	-34.4	0.789	1.72	1.89	1.23	-18.3
20120902346	56173.4891	20	32	10.91	133.2	-185.2	-13.4	1.178	1.74	1.77	1.24	—
20120902347	56173.5032	20	26	10.30	128.7	-184.9	—	1.156	1.74	1.79	1.25	—
20120928444	56198.5006	20	63	10.13	141.3	-198.1	-30.4	0.947	1.74	1.74	1.19	-4.3
20120928445	56198.5156	20	70	10.12	137.6	-193.2	-30.6	0.936	1.71	1.75	1.18	-3.9
2013010357	56296.2614	20	35	9.30	132.2	-200.9	-65.1	0.739	1.66	1.72	1.18	-53.7
2013010358	56296.2755	20	37	9.01	133.3	-206.0	-69.4	0.769	1.64	1.73	1.18	-32.8